J Geophys (1986) 60:139–148

Journal of Geophysics

Original investigations

Deep-seated lateral velocity variations beneath the GRF array inferred from mislocation patterns and P residuals

S. Faber [1], J. Plomerová [2], and V. Babuška [2]

[1] Seismologisches Zentralobservatorium GRF, Krankenhausstraße 1–3, D-8500 Erlangen, Federal Republic of Germany
[2] Geophysical Institute, Czechoslovak Academy of Sciences, 14131 Praha 4, Czechoslovakia

Abstract. The analysis of mislocation patterns and the three-dimensional inversion of travel-time residuals for *P* waves measured at the GRF array reveal the existence of strong lateral velocity variations beneath the array. The most expressive phenomenon consists of an increase of *P*-wave velocities in the upper mantle from north to south, in addition to a possible thickening of the lithosphere to the south; especially the Moldanubian part of the Bohemian massif located to the southeast of the GRF array is characterized by high *P*-wave velocities in the upper mantle. The systematic change of the magnitude of the residual variation across the array, depending on the incidence angle for *P* waves, leads to the conclusion that a low-velocity zone exists in the upper mantle to the northeast of subarray A. The appearance of low-velocity material in the vicinity of the border between the two tectonic units, namely the Saxothuringian zone to the north and the Moldanubian zone to the south, might be connected to the deep structure of the graben area which extends to the northeast into the Egergraben.

Key words: GRF array calibration – Mislocation vectors – *P*-wave trave-time residuals – 3-D inversion – Lateral velocity variations

Introduction

Since the installation of large-aperture seismic arrays within the last 20 years, numerous investigations have dealt with slowness and azimuth anomalies as well as with azimuthal variations of *P*-wave travel-time residuals observed at these arrays. These deviations of measured parameters from theoretical values calculated for standard earth models are due to lateral variations in structures located in most cases in the crust and upper mantle underneath these seismograph networks. This is shown, for example, in an investigation presented by Berteussen (1976), who refers to a number of publications concerning these problems at arrays such as LASA, NORSAR, YKA and others. Aki et al. (1976, 1977) applied a three-dimensional inversion technique to *P*-wave residuals observed at LASA and at NORSAR, respectively. In both cases the results show that strong small-scale inhomogeneities exist down to the bottom of the lithosphere. In a more recent paper, Christofferson and Husebye (1979) located such heterogeneities at NORSAR at even slightly greater depth. As a comparison to the relatively strong heterogeneous media beneath most of the seismic arrays, the Gauribidamur array in India should be mentioned because it seems to have an exceptionally homogeneous lithospheric structure underneath it (Berteussen et al., 1977; Ram and Yadav, 1980).

In our paper we present a study of the mislocation patterns and azimuthal variations in *P*-wave residuals at the broad-band seismic array Gräfenberg (GRF) in the Federal Republic of Germany. A detailed description of the GRF-array configuration is published by Harjes and Seidl (1978). The GRF array is located on a predominantly homogeneous geological surface structure, namely, the Franconian Jurassic limestone formation (Fig. 1). This area, which forms the eastern part of the South German block, is bordered by the Bohemian Massif to the east. The two blocks are separated by zones of fracturing which strike NW. The northern part of the Bohemian Massif is subdivided by ENE-striking zones with Cenozoic volcanism. The boundary between two Hercynian units, the Moldanubian zone in the south and the Saxothuringian zone in the north, crosses the GRF array approximately between subarray A and subarray B with a NE strike (Geologische Karte von Bayern 1:500,000, 1981; Jacobshagen, 1976).

According to the evaluation of seismic refraction data in the array siting area (Aichele, 1976; Giese, 1976a, b; Strößenreuther, 1982), the crustal thickness beneath the GRF array has a constant value of approximately 28–30 km, while it increases to the east beneath the Bohemian Massif. While the crust-mantle boundary in the Moldanubian zone was found to be rather sharp, a change occurs to the NE of the array, entering the Saxothuringian zone where this boundary is less clearly developed and where the top of the upper mantle is characterized by a strongly reduced velocity (Giese, 1976b). Babuška et al. (1984, 1986) used *P* arrival times published in ISC bulletins for central European stations to study *P*-wave travel-time residuals at these stations. For GRF station A1 they calculated a representative average residual of 0.5 s and deduced a subcrustal lithospheric thickness of about 80 km. Raikes and Bonjer (1983), in their study of *P* residuals recorded in the Rhenish massif, included a small number of events recorded at the GRF array and inferred from these data a region of anoma-

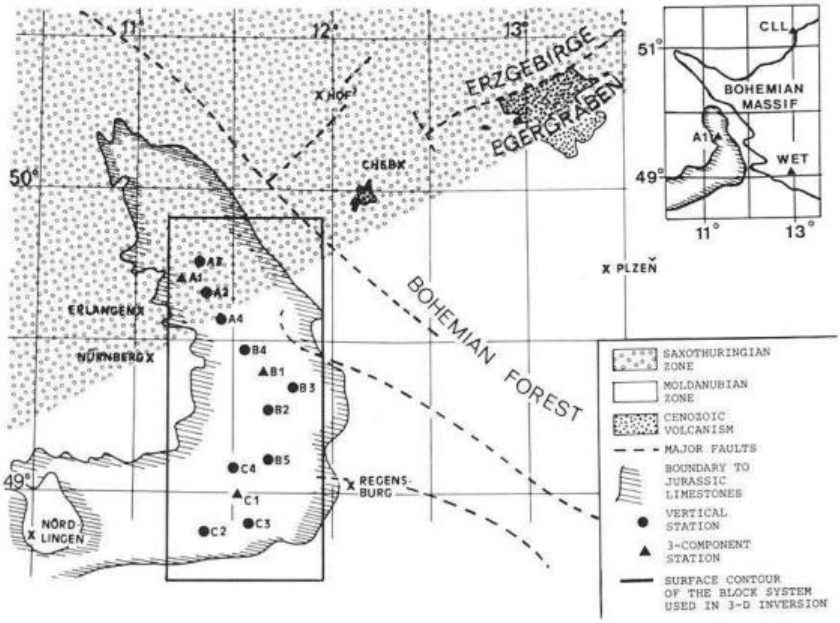

Fig. 1. Location of the GRF array with respect to the geotectonic surrounding. The contour of the block system used for the 3-D inversion is shown. *Upper right*: locations of the stations WET and CLL used as normalizing stations in the 3-D inversion

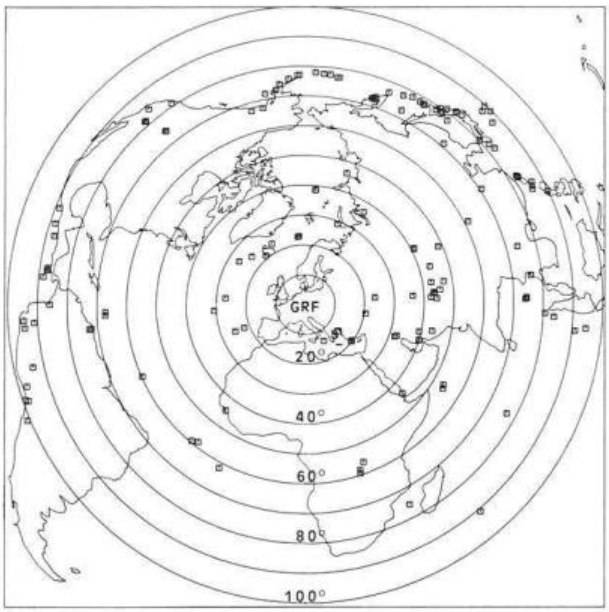

Fig. 2. Distribution of teleseismic events used in the analysis. Epicentral distances are given in degrees from GRF station A1

lously low velocity which extends to a depth of 200 km to the northeast of the array. The existence of deep-seated structures with relatively low velocities located in the northeastern part of the GRF array is also required for the interpretation of the data used in our analysis.

GRF-array mislocations

Mislocation pattern

The most important task in compiling a data base for location calibration is to cover slowness space as densely as possible with mislocation vectors. Departure from an ideal coverage is of course unavoidable since seismic zones on the earth are not homogeneously distributed. Locations of epicentres used in this study are plotted in Fig. 2; epicentral distances range from 20° to 100°. Due to the location of the GRF array relative to the zones of seismic activity, southern azimuths are poorly covered with data. By the term "azimuth", we mean the station-to-source azimuth throughout this paper.

Figure 3 shows the GRF whole-array diagram which represents the mislocation vectors in slowness space. The theoretical and observed values of the slowness $dT/d\Delta$ versus azimuth are drawn as the heads and tails, respectively, of these vectors. Theoretical values have been determined from the USGS hypocentre parameters and a radially symmetric earth model (Jeffreys-Bullen tables). The observed values have been calculated by least-squares fitting of a plane wavefront to the time delays measured at the array stations. Relative onset times were determined by reading the first peak in the signal; this was found to be more accurate than picking first onset times, provided that the signal shape does not change across the array. This was ensured by imposing the restriction of high signal-to-noise ratio and high spatial coherency on the signals of the selected data. Before the relative onset times were determined, the digital broad-band data were filtered to simulate short-period WWNSS seismograms. This procedure produced narrow-band signals and hence sharp peaks such that the error in picking times did not exceed one digitization interval of 0.05 s.

The mislocation vectors are remarkably consistent in orientation and magnitude within large azimuthal ranges (Fig. 3). This observation leads to the assumption that mislocations are not caused by inhomogeneities near the focus or along the deep mantle path of the waves, but that they are due to lateral velocity variations in the array siting area. The variation in magnitude of the slowness and azimuth anomalies can not be correlated with the changes of slowness and azimuth resolution due to the array configuration. The slowness resolution is best at 165° and 345°, while the azimuth resolution is best at 75° and 255° (D. Seidl, personal communication). Generally, vectors point in the direction of lower velocity; for waves approaching from the west and from north to east, the vectors tend to point north- to northeastward. This trend sometimes changes for larger

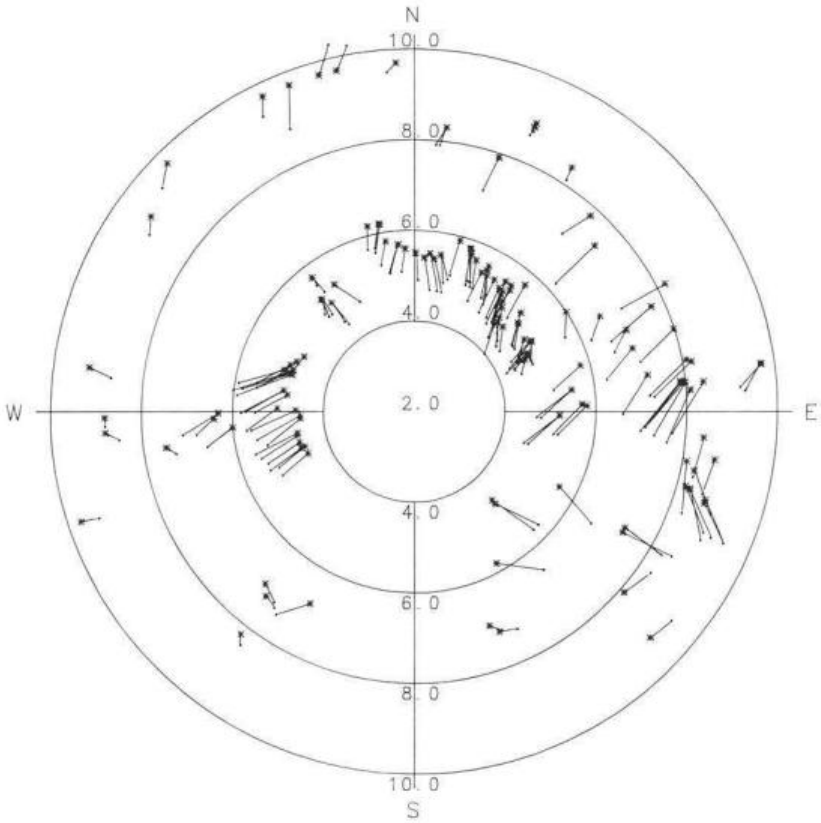

Fig. 3. GRF array diagram for all stations, including mislocation vectors plotted in slowness space. The radial component represents slowness in s/deg. The tail of each vector (•) gives the observed value, while the head (*) represents the PDE solution

incidence angles (high slowness values) as in the case of western azimuths, for instance. This particular change of magnitude and orientation of mislocation vectors, for higher slowness values at certain azimuths, indicates the presence of shallower local velocity perturbations which are sensed by waves depending on their angle of incidence and which are superimposed on the large-scale regional anomaly. Mislocation vectors for waves incident from the southeast and northwest show different behaviour when their orientation is compared to that at other azimuths, suggesting large-scale changes different from those in the northeastern and southwestern quadrants of the array diagram in Fig. 3.

Interpretation

A systematic change in structure (dipping layer or constant lateral velocity gradient) beneath an array will cause a deviation of observed slowness and azimuth from theoretical values which will usually be a periodic function of azimuth. This azimuthal dependence of the slowness and azimuthal anomalies shows up clearly in Fig. 4 which is another presentation of the parameters plotted in Fig. 3. The slowness anomaly is clearly negative for northern azimuths and positive for southern azimuths, with zero crossings close to east and approximately at WNW. For the azimuthal deviation, one zero crossing takes place near north, while the other one is less clear, especially since the data distribution is rather sparse for southern directions. Strong lateral variations of smaller dimension than the systematic change in structure, as they occur to the southeast for instance (Fig. 3), can produce a change of sign at other positions than that caused by the main anomaly. Neglecting for the moment the data points in the southeast and considering

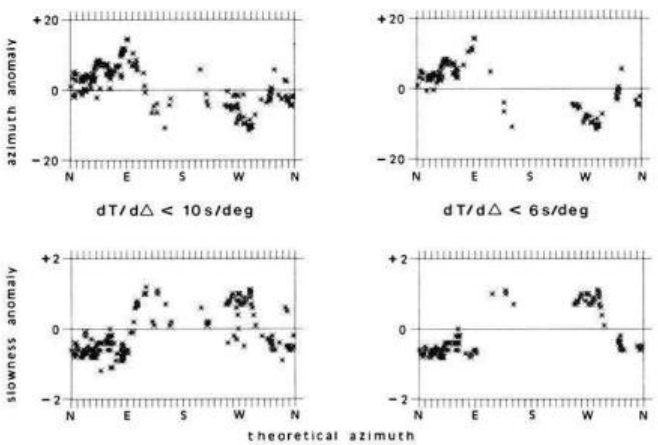

Fig. 4. Observed minus calculated (PDE) azimuth (*top*) and observed minus calculated slowness (*bottom*) as a function of calculated azimuth. The diagrams *on the left* include data for slowness values up to 10 s/deg, while *on the right* only data for slowness values below 6 s/deg are plotted

the fact that the main extrema of the azimuthal anomaly exist in the east (positive) and in the west (negative), a second zero crossing occurs close to south.

Similar azimuthal dependence of slowness and azimuth deviations have been modelled by dipping boundaries between layers of different velocities (Berteussen, 1974; Niazi, 1966; Otsuka, 1966). According to these investigations, the dipping angles and directions of inclined interfaces can be inferred from the position of zero crossings and extrema in azimuthal anomalies. Applying this to the azimuthal anomaly of the GRF array, a dipping interface beneath this area would strike in an east-west direction and dip

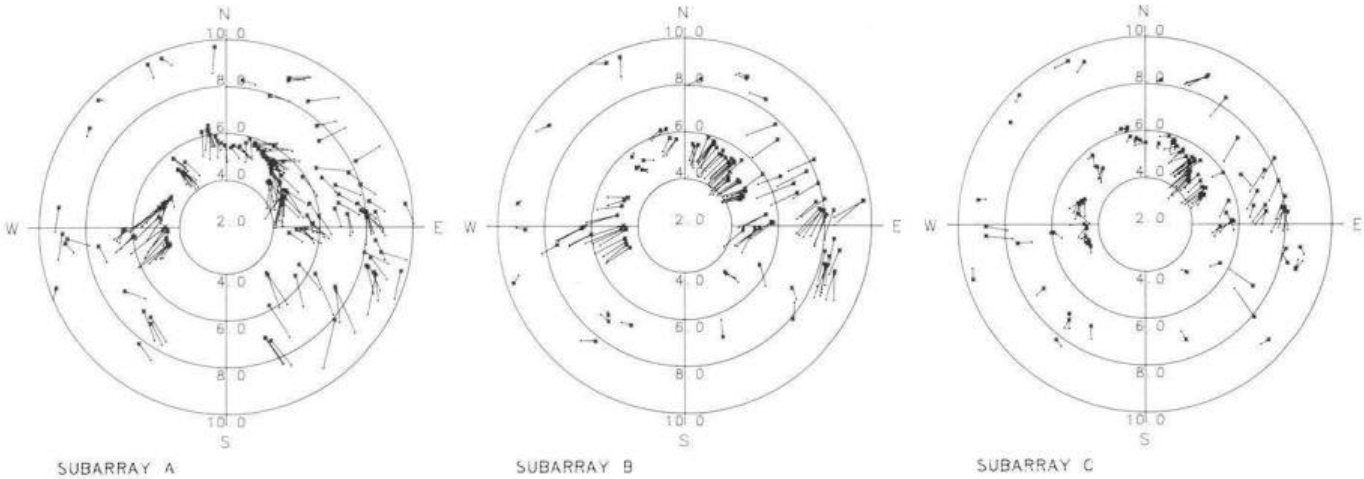

Fig. 5. Mislocation diagrams for single subarrays (for explanation of notations and symbols, see Fig. 3)

northwards in the case of a velocity increase downward across it, while it would dip southwards in the case of a velocity decrease. The dip angle can be approximated from the magnitude of the slowness anomaly, which depends on the angle of incidence under which the wavefront hits the dipping interface (Niazi, 1966). This is one reason for the reduction of scatter in the right part of Fig. 4 which only includes data for slowness values below 6 s/deg, corresponding to an incidence angle at the top of the upper mantle of about 24°. The mean magnitude of the slowness anomaly is approximately 0.8 s/deg. Regarding the relatively constant thickness of the crust beneath the GRF array deduced from refraction seismic measurements (Aichele, 1976; Giese, 1976a, b; Strößenreuther, 1982), the possibility of a strongly dipping crust-mantle boundary must be rejected; a northward dip with an angle of at least 13° would be required to explain the slowness anomaly.

Another possibly dipping interface to be taken into consideration is the lithosphere-asthenosphere boundary. The velocity decrease downwards across it requires a southward dip according to the azimuthal anomaly. The direction of dip would correspond to that deduced for this region from *P*-wave travel-time residuals by Babuška et al. (1986). Nevertheless, the magnitude of the slowness anomaly would require a dip angle of nearly 50°, assuming a velocity decrease from 8.3 km/s to 7.9 km/s at the lithosphere-asthenosphere boundary. Even if we accept a slightly dipping MOHO discontinuity with an angle of at most 2°–3°, not to contradict previous investigations, the required remaining dip of the lithosphere-asthenosphere boundary would still be unrealistically large. From these approximations, it must be concluded that, in addition to a possible southward dip of the lithosphere-asthenosphere boundary, a lateral increase in upper-mantle velocities from north to south is required to explain the relatively large mislocations observed at the GRF array.

Another possibility to be considered is that these anomalies might be partially due to deep-seated abrupt lateral changes in structure, in contrast to the continuous variations across the array examined up to now. Mislocation vectors for the whole-array diagram (Fig. 3) represent average measurements of wavefront distortions across the whole array. Therefore, details in the anomaly pattern, e.g. local structural effects, could be hidden or smeared over all of the array. As a matter of fact, the array diagrams for other station combinations, other than the whole array, reveal that mislocation patterns change with station configuration. Figure 5 shows the mislocation patterns for each subarray. The method and accuracy for the determination of the mislocation vectors has been discussed in connection with Fig. 3. Especially for waves incident from northeastern directions at subarray A, the orientations of mislocation vectors deviate largely from those at subarrays B and C; while for steep incidence from western directions at subarray C, mislocation vectors are substantially shorter than at subarrays A and B. At this point we would like to postpone the discussion on continuous and abrupt changes in velocity contrasts beneath the GRF array till later, since the *P*-wave travel-time residuals supply additional information concerning this problem.

P-wave travel-time residuals

Data

The events selected for the analysis of *P*-wave travel-time residuals were the same as those used for generating the mislocation vectors. The accuracy of the picked arrival times is the same as discussed above. As a first step, the *P* residuals for each station were determined by subtracting the *P* travel times through the Jeffreys-Bullen model from the observed *P* travel times using USGS hypocentral parameters. The effects on *P* residuals which arise from hypocentre mislocations and errors in origin time, as well as from lateral velocity variations in focal regions and along the deep mantle path of the waves, are largely eliminated by normalizing the data for each event. Normalizations are sometimes calculated with respect to the average residual of a station network. However, the interpretation of the mislocation patterns for the GRF array showed that large lateral velocity variations exist beneath the array which would affect the relative residuals considerably if the average is used as a normalization base. Therefore, we chose reference stations situated outside the station area. The location of these normalizing stations should not be too far from the territory under investigation in order to guarantee that the travel paths of the waves in the focal region and in the deeper mantle are about the same for the normalizing

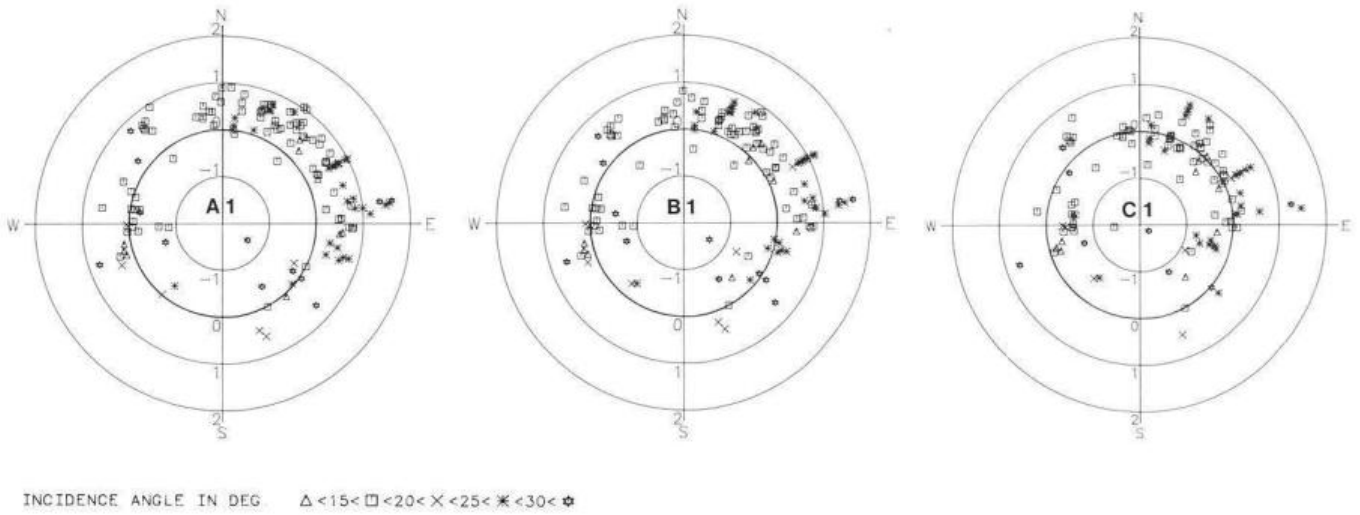

Fig. 6. *P* travel-time residuals for subarray-centre stations A1, B1, C1 calculated for each event relative to the respective mean residual of the normalizing stations WET and CLL. Symbols differ for different intervals of the theoretical incidence angle of *P* waves at the surface. The radial component represents the residuals from −2 s to +2 s

stations as for other stations. It is also important not to impose the effect of structure beneath the normalizing stations onto the data set to be investigated.

According to the patterns of azimuthal variations of *P* residuals at central European stations (Babuška et al., 1984), no single nearby station exists which would be ideal to use as a normalizing station. Therefore, we use the average residual of two stations with nearly opposite patterns in their azimuthal variation of residuals (Babuška et al., 1984) for the present normalization; expecting thus to cancel to a large extent, the structural effects under the normalizing stations. The two selected stations are Wettzell, (WET) located in the Moldanubian zone, and Collm (CLL) in the Saxothuringian zone (Fig. 1). We considered using an average of residuals from more than two stations to further minimize local structural influences, but this would have resulted in a considerable loss of data, since only such events from which onsets were reported at all of the normalizing stations could be used. The onsets at WET and CLL of the events selected in our study were read from station reports to ISC.

Figure 6 shows the *P* residuals for the GRF subarray-centre stations normalized to the average of the residuals of the corresponding events at WET and CLL. While the scatter in the *P* residuals due to errors in hypocentre determinations and in structural contrasts near the focus and in the deeper mantle should be largely eliminated by the applied normalization, we suppose that the scatter in the data of Fig. 6 is partially due to errors in reading onsets at normalizing stations which might sometimes be larger than those at the GRF stations, but also due to local structural variations beneath these stations. Since the onset times at normalizing stations were picked from bulletin reports it is difficult to estimate their accuracy, but we suppose that the errors in reading are not much larger than 0.1 s as we selected events with high-quality signals at the GRF stations. Despite the remaining scatter, the residual patterns (Fig. 6) reveal that a general shift of residuals of about 0.5 s takes place from north (station A1) to south (station C1) and for some azimuths, like ESE, it is even larger.

In order to demonstrate more clearly the change of residuals as a result of lateral inhomogeneities beneath the GRF array and to perform a 3-D inversion, for stability comparisons, based only on the homogeneous data set of the GRF stations, we normalized the data set to one of the array stations, namely to A1. Since the error in picking onset times by doing this is not larger than 0.05 s also for the normalizing station A1, we end up with a minimum of scatter in Fig. 7 and the systematic changes in *P* residuals across the array show up clearly. Choosing A1 as the normalizing station in this case does not imply that the residuals at A1 are less affected by velocity perturbations due to structural inhomogeneities than at other stations of the array. Rather, since A1 is the most reliable station as regards operational time, we picked it in order to obtain as large a data set as possible. Looking at Fig. 7 one has to keep in mind the residual pattern at A1 with respect to the normalizing stations WET and CLL (Fig. 6), A1 being late by an average of 0.5 s from northwestern to eastern directions and just about "normal" for southeastern directions. Figure 7 demonstrates a strong shift in the residuals to negative values, from the northern station A3 to the southern station C2 (Fig. 1), and which is largest for eastern azimuths. For some directions the magnitude of the residual variation is strongly dependent on the incidence angle. From northern to northeastern azimuths, the shift for shallow incidence is small compared to steep incidence. Also, for waves arriving from the east at the southern stations B5 through C4, the shift is largest for angles of incidence between 25° and 30°, namely almost −1 s. A similar phenomenon occurs for southeastern azimuths where the residuals at the stations of subarray B differ by up to 0.5 s (at B3) for various angles of incidence.

3-D inversion of P residuals

Using the standard Aki three-dimensional velocity inversion scheme (Aki et al., 1976, 1977), an automatic inversion was applied to the *P* residuals presented earlier. In this procedure the region beneath the investigated area is divided into several layers, each layer consisting of a system of rectangular blocks. The linear 3-D inversion procedure

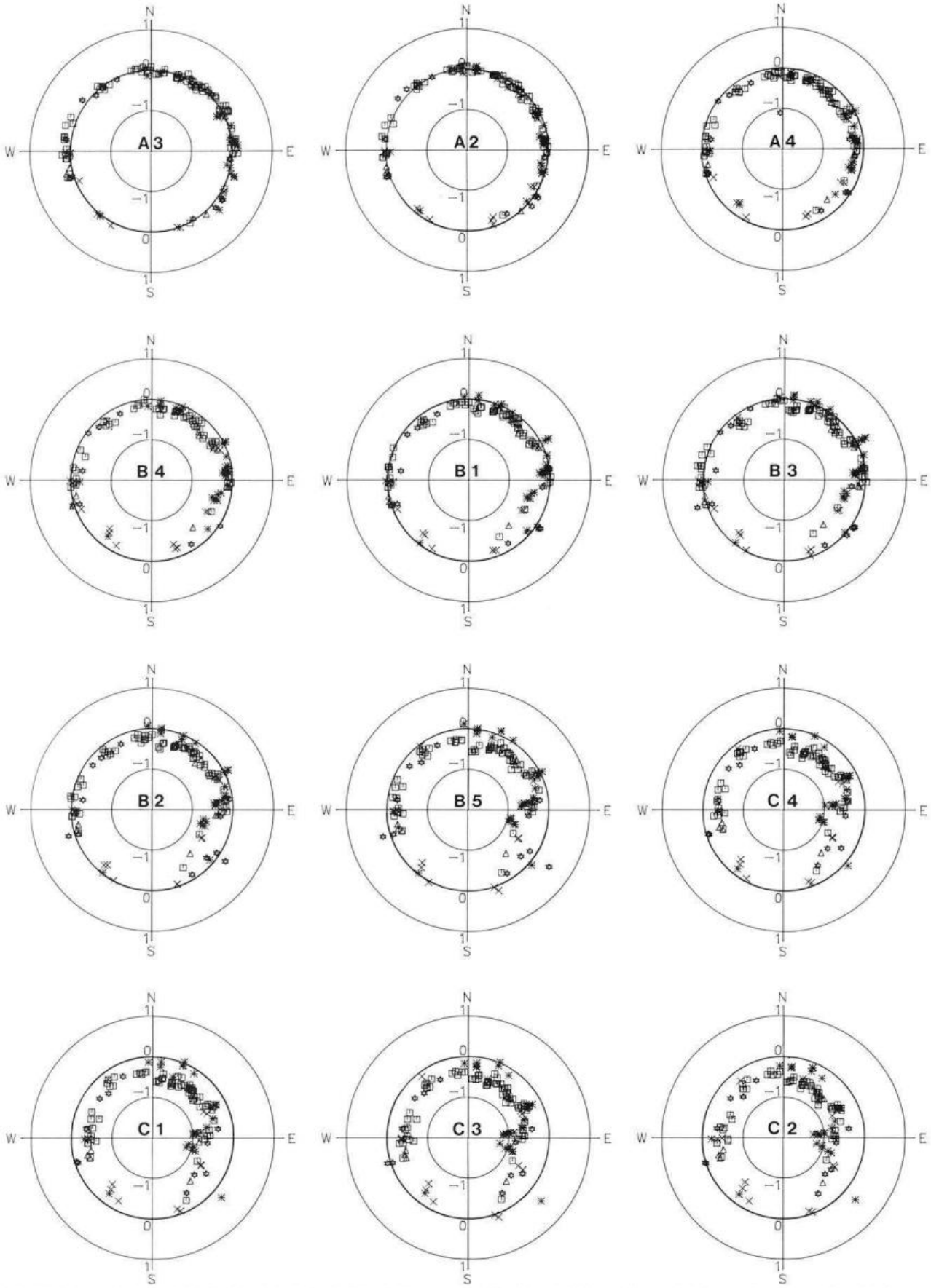

Fig. 7. *P* travel-time residuals for all of the GRF stations normalized to A1 for each event (for explanation of symbols, see Fig. 6). Stations are arranged from left to right and from top to bottom according to their geographic order from north to south

used in this study makes several approximations which severely bias the solution. The principal assumptions of the method are that in each layer a seismic ray propagates only in one single block, namely in that one in which the ray spends most of its time, and that refractions of the ray at the discontinuities between adjacent blocks are neglected. These approximations result in a degradation of the spatial resolution and in an underestimation of velocity perturbations (Koch, 1985). Moreover, the problem of the optimal choice of the block geometry and layer thickness for the reconstruction of an unknown model is difficult to solve without good knowledge of the tectonics and geology of the deep structure to be modelled.

In order to test the influence of the starting model and of the block size as well as of the normalization on the results, the inversion was performed for two different initial 5-layer models (Table 1) and for several block configurations using two sets of input data with different normalizations. The main differences between the two initial models exist in the lower lithosphere, where model 1 includes a velocity decrease from 8.4 km/s to 7.9 km/s at a depth of 79 km, while the velocity-depth function in the uppermost mantle of model 2 represents a gradual increase in velocity from 8.15 km/s at a depth of 30 km to 8.3 km/s at a depth of 130 km. A set of calculations with different damping parameters θ^2 was performed in order to find an acceptable trade-off between the resolution and the stability of the solution. The damping parameter θ^2 is conveniently expressed as $\theta^2 = F^*\max(A^TA)$, $\max(A^TA)$ being the largest diagonal element of the normal equation matrix and F the effective smoothing parameter (Hovland et al., 1981). Figure 8 represents the RMS velocity perturbations versus residual variance improvement for different parameters F ranging from 10 to 0.0001. The parameter 0.05 was adopted for further calculations, because the RMS velocity perturbations for lower values of F increases substantially without a considerable increase of the residual variance improvement.

Figure 9 shows the results of the 3-D inversion for the two initial models (Table 1) with layers being divided into 4 × 4 blocks. Each block is 33.2 km in the NS direction and 21.6 km in the EW direction. The contour of the block system is included in Fig. 1. The horizontal coordinates of the centre of the block system are: 49.31° N, 11.56° E. For good resolution, a minimum of ten rays with a homogeneous azimuthal distribution should pass through each block. When dealing with a real data set we must accept that the azimuthal coverage is far from ideal due to the irregular distribution of epicentres (Fig. 2). Due to the shape of the array, five blocks in the first layer of the models are not hit by rays and some of the blocks, namely those close to margins, are poorly resolved. In the deeper layers almost all of the blocks are crossed by rays; however, the resolution decreases because each block is sampled by fewer rays. Similar velocity perturbations were obtained for both models. The variance improvements of both inversions are the same: 36.1% and 36.8% for models 1 and 2, respectively. The same concerns the values of the diagonal elements of the resolution matrix of individual blocks in layers 1–3. The inversion with model 2 as the initial model results in higher values of the diagonal elements of the resolution matrix in layers 4 and 5 compared to the calculation with model 1. The inversion of the data set normalized with respect to the average residual at WET and CLL results

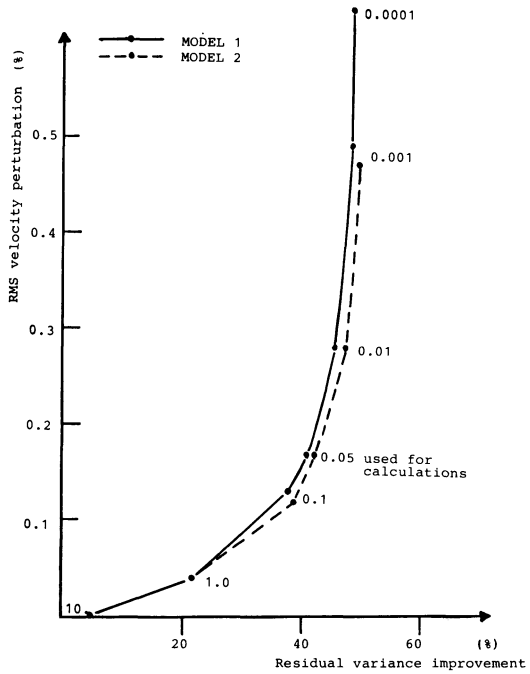

Fig. 8. RMS velocity perturbations versus residual variance improvement, calculated for various values of the effective smoothing parameter F. The computations were done for data normalized to the mean residuals at WET and CLL and for model 1 (*dashed line*) and model 2 (*full line*). The relation between F and the damping parameter θ^2 is given by $F = \theta^2$*max(diagonal element of the normal equation matrix). The value $F = 0.05$ corresponding to $\theta^2 = 224\ s^2$ for model 1 and $\theta^2 = 242\ s^2$ for model 2 was adopted for further calculations

Table 1. Starting models for 3-D inversion

Layer	Thickness (km)		Velocity (km/s)	
	model 1	model 2	model 1	model 2
1	28	30	6.1	6.2
2	26	25	8.2	8.15
3	25	25	8.4	8.2
4	15	25	7.9	8.25
5	26	25	8.1	8.3

in a general increase of velocity from north to south (Fig. 9). The two layers of the uppermost mantle (model layers 2 and 3), especially, are characterized by relatively low-velocity blocks in the northeastern part and by relatively high-velocity blocks to the south, mainly to the southwest.

The 3-D inversion of the P residuals was also computed for the same initial models but for a system of 8 × 8 blocks. The horizontal dimensions of each block were half of those in the 4 × 4 block system. In this case, due to the smaller block dimensions, each block was sampled by a smaller number of rays and the solution became less stable, but the main tendency of the velocity changes across the array was preserved. In order to verify details in the velocity perturbation pattern, we shifted the block system relative to the station locations and recomputed the 3-D inversions; the perturbation pattern was preserved even in detail. These experiments demonstrate that the results of the 3-D inversion concerning the general pattern of velocity perturbations are reliable.

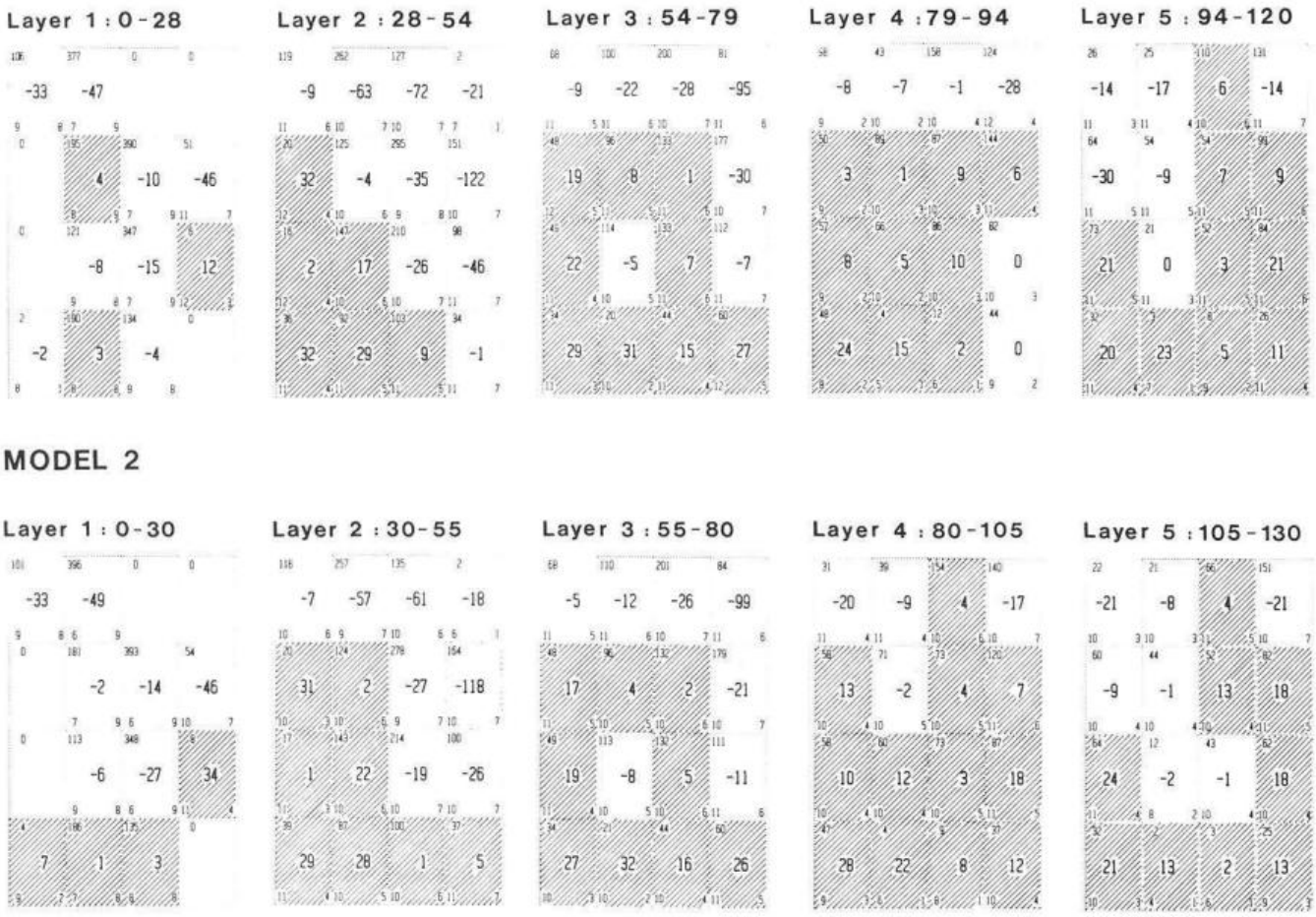

Fig. 9. Velocity perturbations (in tenths of percent of the respective layer velocity of the starting model) obtained by the 3-D inversion of the residuals normalized to WET and CLL. Variance improvements for models 1 and 2 are 36.1% and 36.8%, respectively. The number of rays passing through each block of the 4×4 block approximation of the area is given in the *upper left corner* of each block. The standard errors of the velocity perturbations (in tenths of a km/s) and the values (in tenths) of the diagonal elements of the resolution matrix are plotted in the *left and right lower corners* of each block, respectively. The blocks with positive velocity perturbations are *hatched*

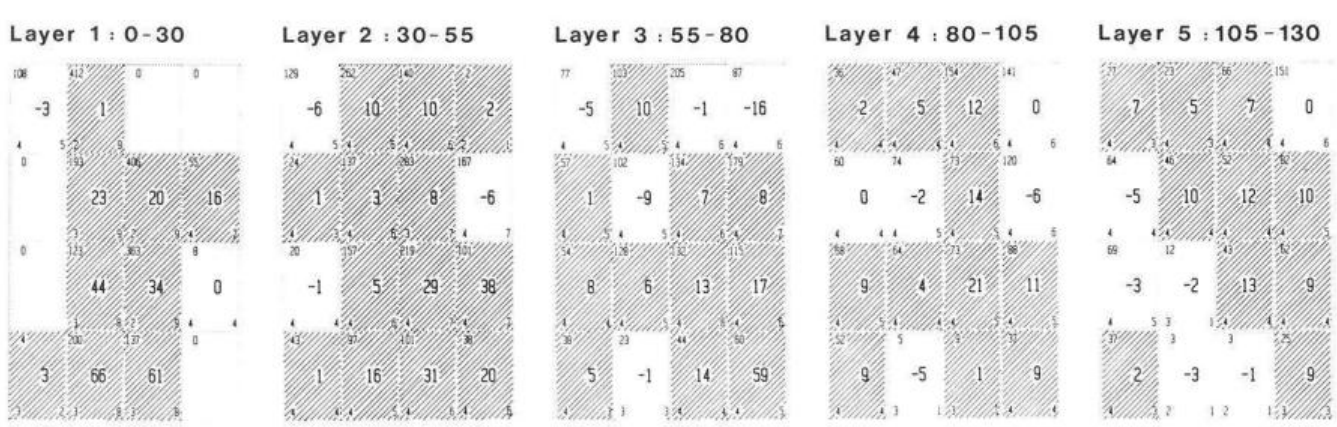

Fig. 10. Velocity perturbations resulting from the 3-D inversion of the residuals normalized to A1 computed for the 4×4 block approximation of the area. The variance improvement is 70% (for notations, see Fig. 9)

3-D inversions were also calculated for a data set normalized to A1 (Fig. 10) in order to check whether the stability of the solution increases if only the uniform data set of the GRF stations is used (Fig. 7). The relatively high value of 70% was obtained for the variance improvement from the inversion of the *P* residuals normalized to A1. Since *P* velocities beneath station A1 are predominantly low (negative velocity perturbations), the inversion of this data set is characterized by high-velocity blocks throughout most of the model. Nevertheless, the change in absolute magnitude of the velocity perturbations from north to south within the individual layers is comparable to that inferred from the data set normalized to the average residual at WET and CLL.

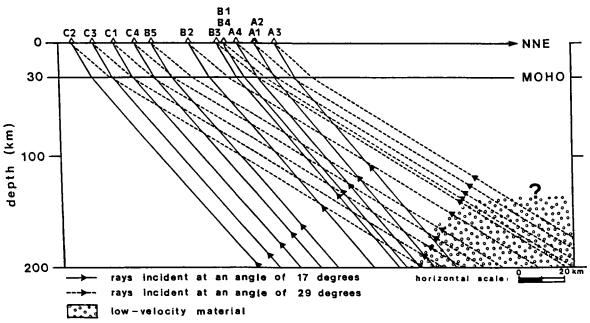

Fig. 11. Schematic ray tracing through a vertical crustal/upper mantle cross-section (simplified model) on a NNE-SSW profile through B1. The locations of the other GRF stations have been projected perpendicularly onto this line. The *question mark* denotes that the upper limit of the low-velocity region is undefined due to the non-existence of stations beyond A3 on this profile

Discussion

The 3-D inversion of the *P* residuals observed at the stations of the GRF array resulted in an increase of velocity from north to south in the uppermost mantle. Considering the reliability of this result, it should, however, be kept in mind that several limitations to the method used for the inversion exist. One of these is that, due to the limited spread of the stations (Fig. 1), the area covered by the block system cannot be extended beyond its present lateral and depth dimensions. This means that the automatic inversion scheme would map velocity perturbations originating from inhomogeneities located outside the block system to the blocks within the system.

The 3-D inversion also produced a velocity decrease from south to north in the crustal layer. A delay of at most 0.1 s in *P* arrival times for the northernmost stations with respect to the southernmost can be explained by changes in sedimentary thicknesses, sedimentary layers being thicker by about 1.5 km in the northernmost part of the array than at the southernmost station sites (Emmert, 1981; Erläuterungen zur Geologischen Karte von Bayern 1:500,000, 1981). After stripping crustal influences, a mean residual variation across the array of about 0.5 s for steep incidence remains, which results in a general increase in velocities from north to south in the uppermost mantle using the 3-D inversion.

A similar effect on *P* residuals, as is produced by a velocity increase within a model with plane horizontal layers, could result from dipping layer boundaries and should therefore be considered. It has been concluded, in an earlier section, that the dipping angles of the crust-mantle or lithosphere-asthenosphere boundary, which would be required to explain the observed deviations in mislocations or the changes in residuals across the array by dipping layer boundaries only, are much too large to be realistic. Moreover, a southward dip of the lithosphere-asthenosphere boundary could not, by itself, produce as large a separation in residuals as a function of incidence angle as is observed across the GRF array, especially for northeastern azimuths. This observation points to another mechanism in addition to the gradual change in structure.

A deep-seated low-velocity region located to the northeast of the array would explain the differentiation of residuals as a function of incidence angle for northern to northeastern azimuths (Fig. 11). It is obvious that such a low-velocity zone cannot be located in the lithosphere directly beneath the stations, but has to be sought for at least at a distance from the array where the waves incident at steeper angles are seperated enough from those with shallow incidence to produce the observed phenomenon (Fig. 7). In such a case the low-velocity region would be sensed across the whole array by rays incident at large angles from NNE, but would not influence the travel times of rays with steep incidence except at the northernmost stations. The location of this region is not, or only marginally, included in the block system set up for the inversion. Considered in terms of structural variations related to tectonic features, it must be kept in mind that the boundary between two geological units, the Saxothuringian zone in the north and the Moldanubian zone in the south, crosses the investigated region approximately between the subarrays A and B with an ENE strike (Fig. 1). A low-velocity material appearing as an asthenolith in the vicinity of this boundary between the two geological units and extending to the ENE, being less pronounced to the WSW, would explain the positive *P* residuals observed at subarray A as well as the differentiation of residuals as a function of incidence angle crossing the array from north to south. It has already been mentioned in an earlier section that the mislocation pattern of subarray A differs largely from those of the other two subarrays B and C, especially for northeastern azimuths, and this could also be explained by such a velocity anomaly. This supports the hypothesis that structures do not vary gradually from north to south across the array, but that the northeastern part is anomalously slow with a rather abrupt change to the south.

Besides the model specifications discussed up to now, the structures beneath the Moldanubian part of the Bohemian Massif seem to include very high velocities sensed by rays incident to subarrays B and C from eastern to southeastern directions. Mislocation vectors for these azimuths also indicate an increase in velocities. This pronounced velocity increase to the southeast of the array might be related to directional variations of velocities (anisotropy) within the lower lithosphere as well as to an increase in lithospheric thickness underneath the southern part of the Bohemian Massif. Refraction seismic studies in the southwestern part of the Bohemian Massif have shown a crust-mantle boundary dipping steeply from the SW to the NE underneath the Bohemian massif (Strößenreuther, 1982). As had been outlined before, the change in residuals discussed here is again coupled to a clear differentiation of their magnitude as a function of angle of inci-

dence, being strongest for subarray B from southeastern azimuths and for subarray C from eastern azimuths (Fig. 7). This dependence of the magnitude of the residuals on the angle of incidence leads to the conclusion that the velocity perturbations or lateral changes in structure causing this effect are located not directly beneath the stations but at some distance to the ESE in the upper mantle.

Summary

Strong lateral variations definitely exist in the uppermost mantle beneath the GRF array. The general feature is a deep-seated velocity increase from north to south, i.e. from the Saxothuringian zone into the Moldanubian zone, superimposed on the effect of a possible thickening of the lithosphere from north to south as has been derived by Babuška et al. (1986). This is inferred from the interpretation of the whole-array mislocation pattern as well as from the gradual decrease of *P* residuals from north to south across the array and from their differentiation as a function of incidence angle. A low-velocity zone located in the upper mantle to the NE of the array close to the transition region from the Saxothuringian into the Moldanubian zone might be connected to the deep structure of the Egergraben. This region is characterized by Cenozoic volcanism (Fig. 1) and by an increase in heat flow (Čermák and Hurtig, 1979) which might be coupled to the low-velocity material inferred from the *P* residuals. In contrast to these low-velocity structures in the north, the Moldanubian part of the Bohemian Massif which has been sampled by our data reveals very high velocities in the uppermost mantle.

Acknowledgements. We are indebted to U. Achauer and J. Šílený for providing programs and support in computing. We would like to thank U. Achauer, B. Buttkus and D. Seidl for critically reading the manuscript and for numerous helpful discussions. We appreciate very much the translation assistance and comments given by M. Hellweg. The present investigation was supported by the Deutsche Forschungsgemeinschaft (German Research Council) under contracts SZ32/6-1 and AI12/1-2 and partially by UNESCO under contract SC/RP 590992. The Gräfenberg array is part of the Bundesanstalt für Geowissenschaften und Rohstoffe (Federal Institute for Geosciences and Natural Resources) and is supported by the Deutsche Forschungsgemeinschaft.

References

Aichele, H.: Interpretation refraktionsseismischer Messungen im Gebiet des fränkisch-schwäbischen Jura. Ph.D. thesis, University of Stuttgart, 1976

Aki, K., Christofferson, A., Husebye, E.S.: Three-dimensional seismic structure of the lithosphere under Montana LASA. Bull. Seismol. Soc. Am. **66**, 501–524, 1976

Aki, K., Christofferson, A., Husebye, E.S.: Determination of the three-dimensional seismic structure of the lithosphere. J. Geophys. Res. **82**, 277–296, 1977

Babuška, V., Plomerová, J., Šílený, J.: Large-scale oriented structures in the subcrustal lithosphere of Central Europe. Ann. Géophys. **2**, 649–662, 1984

Babuška, V., Plomerová, J., Šílený, J.: Structural model of the subcrustal lithosphere in Central Europe. In: The composition, structure and dynamics of the lithosphere-asthenosphere system, C. Froidevaux and K. Fuchs, eds. 1986 (in press)

Berteussen, K.A.: NORSAR location calibrations and time delay corrections. Scientific Report No. 2-73/74, NTNF/NORSAR, 1974

Berteussen, K.A.: The origin of slowness and azimuth anomalies at large arrays. Bull. Seismol. Soc. Am. **66**, 719–741, 1976

Berteussen, K.A., Husebye, E.S., Mereu, R.F., Ram, A.: Quantitative assessment of the crust – upper mantle heterogeneities beneath the Gauribidamur seismic array in southern India. Earth Planet. Sci. Lett. **37**, 326–332, 1977

Čermák, V., Hurtig, E.: Heat flow map of Europe 1:5,000,000. In: Terrestrial heat flow in Europe, Čermák, V. and Rybach, L., eds. Berlin, Heidelberg, New York: Springer-Verlag 1979

Christoffersson, A., Husebye, E.S.: On three-dimensional inversion of P wave time residuals: option for geological modeling. J. Geophys. Res. **84**, 6168–6175, 1979

Emmert, U.: Die Fichtelgebirgsschwelle an der Fränkischen Linie. Jber. Mitt. oberrhein. geol. Ver. **63**, 219–228, 1981

Erläuterungen zur geologischen Karte von Bayern 1:500,000, (3. Auflage). Bayer. Geol. Landesamt, München, 1981

Geologische Karte von Bayern 1:500,000, (3. Auflage). Bayer. Geol. Landesamt, München, 1981

Giese, P.: Models of crustal structure and main wave groups. In: Explosion seismology in Central Europe, Giese P. et al., eds.: pp. 196–200, Berlin, Heidelberg, New York: Springer-Verlag 1976a

Giese, P.: The basic features of crustal structure in relation to the main geological units. In: Explosion seismology in Central Europe, Giese P. et al., eds.: pp. 221–241, Berlin, Heidelberg, New York: Springer-Verlag 1976b

Harjes, H.-P., Seidl, D.: Digital recording and analysis of broadband seismic data at the Graefenberg (GRF)-array. J. Geophys. **44**, 511–523, 1978

Hovland, J., Gubbins, D., Husebye, E.S.: Upper mantle heterogeneities beneath Central Europe. Geophys. J.R. Astron. Soc. **66**, 261–284, 1981

Jacobshagen, V.: Main geologic features of the Federal Republic of Germany. In: Explosion seismology in Central Europe, Giese P. et al., eds.: pp 3–17, Berlin, Heidelberg, New York: Springer-Verlag 1976

Koch, M.: A numerical study on the determination of the 3-D structure of the lithosphere by linear and non-linear inversion of teleseismic travel times. Geophys. J.R. Astron. Soc. **80**, 73–93, 1985

Niazi, M.: Corrections to apparent azimuths and travel-time gradients for a dipping MOHOROVICIC discontinuity. Bull. Seismol. Soc. Am. **56**, 491–509, 1966

Otsuka, M.: Azimuth and slowness anomalies of seismic waves measured on the central California seismographic array. Part II. Interpretation. Bull. Seismol. Soc. Am. **56**, 655–675, 1966

Raikes, S., Bonjer, K.-P.: Large-scale mantle heterogeneity beneath the Rhenish Massif and its vicinity from teleseismic P-residuals measurements. In: Plateau uplift, K. Fuchs et al., eds.: pp 313–331, Berlin, Heidelberg, New York: Springer-Verlag 1983

Ram, A., Yadav, L.: Evidence for upper mantle heterogeneity around 650 km depth beneath the Indian subcontinent. Tectonophysics **68**, 17–23, 1980

Strößenreuther, U.: Die Struktur der Erdkruste am Südwest-Rand der Böhmischen Masse, abgeleitet aus refraktionsseismischen Messungen der Jahre 1970 und 1978/79. Ph.D. thesis, University of Munich, 1982

Received January 3, 1986; revised version July 3, 1986
Accepted September 1, 1986